# Stereospecificity and Enantioselectivity in the Binding of the Platinum(II) Complex [$PtCl_2$(tmdz)] (tmdz = 5,5,7-Trimethyl-1,4-diazacycloheptane) to Dinucleotides and Oligonucleotides

**Vivienne P. Munk,[a] Connie I. Diakos,[a] Barbara A. Messerle,[b] Ronald R. Fenton,[a] and Trevor W. Hambley*[a]**

**Abstract:** The two stereoisomers formed on reaction of each of the enantiomers of [$PtCl_2$(tmdz)] with d(GpG) have been identified by using one- and two-dimensional $^1$H NMR spectroscopy. For both isomers formed with the *R* enantiomer the 3′-H8 shifts are downfield from those for the 5′-H8. For the *S* enantiomer the reverse is observed, showing that the bulky tmdz ligand determines the pattern of shifts. Models of these isomers generated by molecular mechanics show that the bulky tmdz ligand limits the rotation of the guanine bases and enforces right-handed (R2) canting for both isomers formed by the *R* enantiomer and left-handed (L1) canting for those formed by the *S* enantiomer. The pattern of H8 shifts is the opposite to that expected for these cantings; this suggests that other factors may play a role in determining these shifts. The interactions between the tmdz and d(GpG) ligands are also shown by molecular mechanics and the broadness of the H8 NMR signals to influence the tendency of the coordinated guanine bases to rotate about their Pt–N7 bonds. Reaction of each of the enantiomers with a 52 base-pair nucleotide, with a total of six GpG binding sites, resulted in the formation of only one of the stereoisomers in each case, the first reported case of complete stereoselectivity, or stereospecificity, in the reaction of Pt complexes with DNA. The observed stereoisomers were identified by comparison with the properties of the d(GpG) complexes. Molecular mechanics models of the adducts with duplex DNA show that the nonformation of one stereoisomer is consistent with the steric bulk of the tmdz ligand preventing closure from the monofunctional adduct to the bifunctional adduct. Enantioselectivity is also observed in that the *R* enantiomer forms more monofunctional adducts than bifunctional (59:41), whereas the *S* enantiomer forms more bifunctional adducts (27:73). The origins of this enantioselectivity must be at the level of monofunctional adduct formation and this has been investigated by molecular mechanics modelling.

**Keywords:** DNA · molecular modeling · NMR spectroscopy · platinum · stereospecificity

## Introduction

Platinum-based anticancer drugs such as cisplatin (*cis*-[$PtCl_2(NH_3)_2$]) and BBR3464 ([(*trans*-$PtCl(NH_3)_2)_2${*μ-trans*-$Pt(NH_3)_2(NH_2(CH_2)_6NH_2)_2$}]$^{4+}$) are believed to effect their action by binding to DNA.[1–7] Numerous factors are believed to influence the DNA binding of such compounds including aquation rates, hydrogen bonding, steric interactions and charge.[8–12] For all mononuclear bifunctional platinum(II) complexes whose DNA binding has been studied, the primary binding site is two adjacent guanines on the same strand (GpG),[13–21] and there is increasing evidence that this is the adduct primarily responsible for the anticancer action of such drugs.[1, 22] Therefore, there is great interest in developing an understanding of the factors controlling binding at the GpG site. Unsymmetric or asymmetric compounds that generate two isomers of the GpG adduct are particularly useful in this context, because any stereoselectivity observed in the formation of these isomers can shed light on the factors that control platinum binding to DNA. Only four such compounds have had their binding to duplex DNA studied in detail.[19–21, 23] Of these, *cis*-[$PtCl_2$(cyclohexylamine)($NH_3$)] and *cis*-[$PtCl_2$(2-methylpyridine)($NH_3$)] (AMD473) have chemically inequivalent am(m)ines and, therefore, the observed stereoselectivity might be due to structural effects and/or differences in aquation rates *trans* to the different am(m)ine ligands.[20, 21] In only one case, [$PtCl_2$(hpip)] (hpip = 1,4-diazacycloheptane), which generates two isomeric forms of

[a] Prof. T. W. Hambley, Dr. V. P. Munk, Dr. C. I. Diakos, Dr. R. R. Fenton
Centre for Heavy Metals Research, School of Chemistry
University of Sydney, NSW 2006 (Australia)
Fax: (+61) 2-9351-3329
E-mail: t.hambley@chem.usyd.edu.au

[b] Dr. B. A. Messerle
School of Chemical Sciences, University of New South Wales
NSW 2052 (Australia)

Supporting information for this article is available on the WWW under http://www.chemeurj.org/ or from the author.



0947-6539/02/0823-5486 $ 20.00+.50/0 *Chem. Eur. J.* **2002**, *8*, No. 23

the GpG adduct in a 1:3 ratio, can the observed stereoselectivity be ascribed to structural effects alone.[19] We have identified the isomers found for [$PtCl_2$(hpip)] and recently shown how steric interactions between the DNA and the propylene chain of the ligand give rise to the observed stereoselectivity.[19]

In order to confirm that steric interactions can have a pronounced effect on formation of the adduct GpG adduct, and to establish whether it is possible to achieve complete stereoselective control (i.e., stereospecificity) we have investigated the DNA binding of [$PtCl_2$(tmdz)] (tmdz = 5,5,7-trimethyl-1,4-diazacycloheptane), a bulkier analogue of [$PtCl_2$(hpip)]. The tmdz ligand is chiral; this raises the

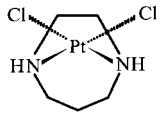


[$PtCl_2$(hpip)]

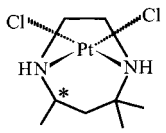


[$PtCl_2$(tmdz)]

additional possibility of enantioselectivity in the adduct formation and thereby, even more detailed insight into steric controls of the adduct formation. Here we describe studies of the formation of the GpG adduct on a 52-mer duplex oligonucleotide by the enantiomers of [$PtCl_2$(tmdz)] and identification of the isomeric forms of the adducts by one- and two-dimensional NMR spectroscopy of the d(GpG) complexes of these enantiomers.

## Experimental Section

**Instrumentation**: High-performance liquid chromatography (HPLC) experiments were carried out by using a Bio-Rad Series 800 HRLC system, with v2.30.1a software, equipped with a Bio-Rad UV-1806 detector, a model AS-100 HRLC automatic sampling system and a model 2800 solvent delivery system. An Alltech Platinum® C-18 column (5 μm particle size, 4.6 × 250 mm) was used for analytical investigations. The preparative column used for large-scale separation was a Waters RCM fitted with a Prep Nova-Pak® HR C-18 cartridge (6 μm particle size, 25 × 100 mm). Platinum concentrations were determined by using a Varian SpectrAA-20 absorption spectrometer graphite furnace, equipped with a GTA-96 graphite tube atomiser and a PC-56 autosampling system. Graphite furnace atomic absorption spectroscopy (GFAAS) readings were measured between 0–302.7 ppb in an HCl matrix. A Braun Christ alpha 1-2 freeze-dryer, fitted to a Javac pump, was used to lyophilise biological samples. NMR spectroscopy was carried out on Bruker DPX400, DMX500 and DMX600 spectrometers, with commercially available solvents (Aldrich or Merck) of 99.6% isotopic purity or better. All two-dimensional $^1$H NMR experiments were carried out on a Bruker Avance DMX 600 MHz spectrometer. Heteronuclear two-dimensional NMR experiments were carried out on a Bruker 500 MHz spectrometer. All spectra were referenced to an internal standard or to solvent isotopic impurities.

**HPLC chromatography**: Platinated/DNA species were analysed by using HPLC performed at a flow rate of 1 mL min$^{-1}$. An organic phase of either HPLC grade methanol or acetonitrile/water (1:1) and an aqueous phase of ammonium acetate (0.1 M, pH 5.5) or triethylammonium acetate (TEAA, Fluka, 0.02 M, pH 7) were used. The elution of DNA fragments was detected using an UV-visible detector set at 254 nm.

**Preparation of [Pt(amine)/dG] and [Pt(amine)/d(GpG)] standards**: The tmdz ligand was resolved and [$PtCl_2$\{(*R*)-tmdz\}] and [$PtCl_2$\{(*S*)-tmdz\}] were prepared as described previously.[24] The preparation of the platinated dG (Sigma) and d(GpG) (Sigma) standards for [$PtCl_2$\{(*R*)-tmdz\}] and [$PtCl_2$\{(*S*)-tmdz\}] were carried out by using a method adapted from published procedures.[14, 25] Platinated/dG samples were prepared by reacting a range of molar equivalents of [$PtCl_2$(amine)] with dG in sodium perchlorate (0.1M, pH 5.5). The monofunctional adducts were prepared by incubating equimolar amounts of freshly dissolved platinum complex and dG at 37 °C for 7 days. The bifunctional adducts were prepared by incubating 2 molar equivalents of dG with the freshly dissolved platinum complex at 37 °C for 7 days. All samples were stored at −20 °C until HPLC analysis. To prepare the bifunctional Pt/d(GpG) adducts, freshly dissolved (*R*)- and (*S*)-[$PtCl_2$(tmdz)] (1.34 mM, 149 μL) were treated with equimolar amounts of d(GpG) (Sigma, 5 mM, 40 μL) in sterile aqueous sodium perchlorate (0.1M, pH 5.5). The samples were incubated at 37 °C for 7 days and stored at −20 °C until required for HPLC analysis.

**Preparation of the stereoisomers of (*R*)- and (*S*)-[Ptd(GpG)(tmdz)] for two-dimensional NMR spectroscopy**: Large-scale samples for acquisition of NMR spectra were prepared by following an adapted literature method.[26] Freshly dissolved solutions of (*R*)- and (*S*)-[$PtCl_2$(tmdz)] (5 mM, 1.294 mL) were treated with equimolar amounts of d(GpG) (5 mM, 1.294 mL). Both reactants were dissolved in sterile aqueous sodium perchlorate, 0.02 M, pH 5.5. The samples were incubated at 37 °C for 7 days and stored at −20 °C prior to HPLC analysis.

**NMR spectroscopy methods**: Experiments were performed by using standard or modified Bruker pulse sequences (XWinNMR, v2.6). One-dimensional $^1$H spectra and two-dimensional DQF-COSY and ROESY spectra were acquired by means of water suppression by pre-saturation, with a recycle delay of 1.81 s used throughout. DQF-COSY spectra were typically collected over a spectral width of 6000 Hz with data sets resulting from 512 increments of $t_1$, with each free induction decay composed of 2048 data points. For each increment of $t_1$, 64 transients were recorded. ROESY spectra of 200 ms mixing time were recorded over a spectral width of 6000 Hz. Data sets resulting from 512 increments of $t_1$ were recorded, with each free induction decay composed of 2048 data points. For each increment of $t_1$, 64 transients were recorded. One-dimensional $^1$H–$^{31}$P correlation spectra were acquired using a standard Bruker pulse sequence over a spectral width of 7000 Hz, with 5000 transients recorded. Spectra were optimised for $J$(H,P) of 3, 5, 7 and 9 Hz.

All spectra were processed by zero filling and subjecting the data to shifted sine-bell weighting functions in $F1$ and $F2$ of π/2, and were baseline corrected by using Bruker XWinNMR software, version 2.6. Spectra were referenced to an internal standard or to isotopic solvent impurities.

**Reactions of platinum complexes with duplex DNA**: A 52 base-pair (bp) self-complementary oligonucleotide of the sequence shown below was treated with the platinum complexes, following a procedure adapted from several literature methods.[16, 17, 27, 28]

5′TAA TTG GTA TAT TGG TAT ATA CCA ATA TTG GTA TAT ACC AAT ATA CCA ATT A 3′

3′ATT AAC CAT ATA ACC ATA TAT GGT TAT AAC CAT ATA TGG TTA TAT GGT TAA T 5′

The oligonucleotide was annealed by using a previously reported procedure.[19] The DNA (1640 μg, Sigma, sodium salt) was dissolved in high purity water (1 mL) and then denatured by heating at 95 °C for 5 min. The oligonucleotide was then slowly renatured by stepwise cooling. The DNA was incubated at 65 °C for 10 min, 37 °C for 30 min, 65 °C for 10 min, 37 °C for 4 h and then slowly cooled to room temperature. The annealed oligonucleotide was stored at −20 °C. The oligonucleotide (100 μg) was incubated for 7 days at 37 °C with freshly dissolved platinum complex (1 mM in 0.02 M $NaClO_4$, pH 5.5, 92.37 μL) at an $R_t$ value of 0.05 (0.9 Pt atoms per GpG site). The platinated DNA was then treated with $P_1$ nuclease (40 μg, Type EC 3.1.30.1 in 50% 20 mM sodium acetate, 50% glycerol solution, pH 5.5, Sigma) at 37 °C for 16 h. Tris buffer (1M, pH 9, 40 μL) was added, and the samples were incubated with alkaline phosphatase (10 U, in 2.5 M ammonium sulfate solution, Sigma) for a further 4 h at 37 °C. The digested DNA was then freeze-dried, resuspended in aqueous sodium perchlorate (0.02 M. pH 5.5, 200 μL) and stored at −20 °C until HPLC analysis.

Platinum profiles of the chromatograms were determined by collecting fractions eluted from the HPLC every 15 s. The platinum content of each fraction was measured by using graphite furnace atomic absorption spectroscopy (GFAAS). Platinated peaks in the chromatogram were

  0947-6539/02/0823-5487 $ 20.00+.50/0 

identified by spiking the digested DNA solution with a small amount of either the platinated/dG or platinated/d(GpG) standard. A procedure adapted from Eastman[14] was used to identify the monofunctional products formed in the reaction between the platinum complexes and the 52-mer. Platinated peaks were incubated at 25 °C for 60 minutes with deionised thiourea (10 mM final concentration) and this produced a change the retention time of monofunctional platinated digested products. Alternatively, platinated peaks in the reaction profile were incubated with 1 M thiourea, cleaving the platinum and leaving the unplatinated DNA fragment in the reaction mixture. The unplatinated nucleotide or dinucleotide was then identified by comparison of the retention time on the HPLC with those of standard nucleotides and nucleosides.

**Molecular modelling**: Starting models for molecular modelling were generated using HYPERCHEM[29] and energy-minimised using MOMECSG-95.[30] The force fields used have been previously published,[31–33] and all models were subjected to energy minimisation using MOMECSG-95 until convergence (all shifts $< 0.01$ Å) was achieved. Minimised strain energies of the dinucleotide complexes are reported in Table 1.

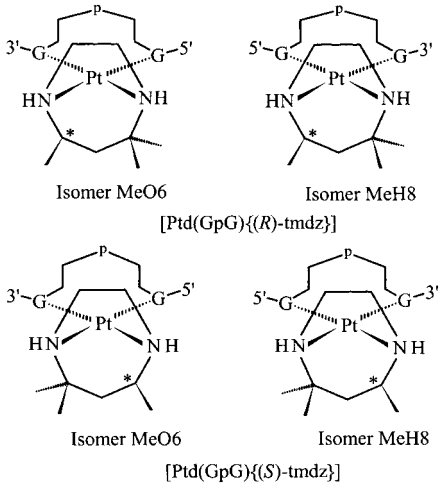


Table 1. Minimised strain energies [kJ mol$^{-1}$] for the enantiomers, isomers and rotamers of [Ptd(GpG)(tmdz)].

| | [Ptd(GpG){(*R*)-tmdz}] | | [Ptd(GpG){(*S*)-tmdz}] | |
|---|---|---|---|---|
| Rotamer | Isomer MeO6 | Isomer MeH8 | Isomer MeO6 | Isomer MeH8 |
| $HH_1$ | − 139.3 | − 145.7 | − 134.6 | − 144.9 |
| $HT_1$ | − 142.0 | − 142.1 | − 151.5 | − 151.5 |
| $\Delta(HT_1 - HH_1)$ | − 2.7 | 2.6 | − 16.9 | − 6.6 |
| $HT_2$ | − 154.2 | − 153.1 | − 149.6 | − 147.3 |
| $\Delta(HT_2 - HH_1)$ | − 14.9 | − 7.4 | − 15.0 | − 2.4 |

Modelling of the duplex structures was carried out by using the sequence: 5′-d($C_1A_2T_3G_4G_5T_6A_7C_8$)-3′:3′-d($G_{16}T_{15}A_{14}C_{13}C_{12}A_{11}T_{10}G_9$)-5′ or the sequence dG8:dC8. The DNA starting models were constructed in HyperChem in a B-DNA conformation and were minimised by using the geometry optimisation routine in HyperChem with the Fletcher–Reeves conjugate gradient method. The bifunctional platinum–oligonucleotide model of the former sequence was constructed by using HyperChem (PC version) and a set of force fields adapted from those provided by Dr. Ulrich Bierbach. The bifunctional adduct was formed by attaching platinum atoms to each of the guanines G4 and G5 at the N7 atoms, at an initial separation of 3.86 Å. The two platinum atoms were brought together in 0.5 Å steps by applying restraints with a force constant of 2800 kJ mol$^{-1}$ Å$^{-1}$, with the energy term removed for the platinum atom in nonbonded interactions and a geometric optimisation routine was used. Upon reaching a separation of 0.5 Å between the two platinum atoms, the 3′-Pt atom was removed and a bond created to join the 5′-Pt to the N7 atom of G5. The platinum energy term was restored, the {Pt(tmdz)}$^{2+}$ moieties docked on and the models minimised using MOMECSG-95 until a difference in total strain energy of less than 1 kJ mol$^{-1}$ occurred between successive minimisation cycles. The dG8:dC8 models were derived from the equivalent models for [$PtCl_2$(hpip)].[19]

## Results and Discussion

**Modelling of the d(GpG) adducts**: When either enantiomer of [$PtCl_2$(tmdz)] binds to the dinucleotide d(GpG), two species are formed in approximately equal amounts and are readily separated by HPLC.[24] These species are referred to as bands 1 and 2 reflecting the order of elution. Variations in the chemical shifts of the H8 atoms of the dinucleotides as a function of pH confirms that in all cases, coordination is through the N7 atoms of the guanine bases (Figures S1 and S2 in the Supporting Information). Thus, the species formed are believed to correspond to the isomers, shown schematically; these differ in respect of the relative orientations of the tmdz and d(GpG) ligands. These isomers are analogous to those formed by [$PtCl_2$(hpip)] and are also expected to form when [$PtCl_2$(tmdz)] binds to duplex DNA. To determine which band corresponds to which isomer, molecular modelling as well as one- and two-dimensional $^1$H NMR spectroscopy were undertaken for each of the two isomers formed by the enantiomers (four isolated complexes). Two head-to-head ($HH_1$ and $HH_2$) and two head-to-tail ($HT_1$ and $HT_2$) conformers of the d(GpG) ligand are possible[34] for each isomer and all were modelled. However, the $HH_2$ forms could not be minimised to a stable geometry, reverting in all cases to a HT form. This is not unexpected as $HH_2$ forms have only been observed with ligands that severely limit rotation about the Pt–N7 bond and/or impose steric constraints.[34]

**Head-to-head models**: Molecular models of the $HH_1$ forms of each of the two isomers for each enantiomer are shown in Figure 1 and reveal significant differences. The conformation adopted by the tmdz ligand in all models is the same as that seen in the crystal structure of [$PtCl_2$(tmdz)].[24, 35] One of the three methyl groups attached to the propylene chain is disposed toward the platinum and, therefore, toward the dinucleotide. This methyl group is hereafter referred to as the axial methyl group. In the $HH_1$ models of isomer MeO6 for both enantiomers, the axial methyl group lies on the same side of the coordination plane as the O6 atoms of the guanine bases, whereas in the $HH_1$ models of isomer MeH8 it lies on the same side as the H8 atoms; this is the basis of the naming of the isomers. The O6 atoms make much more energetically unfavourable contacts with the axial methyl group than do the H8 atoms and consequently the strain energies of the isomers MeO6 are significantly higher than those of isomers MeH8 (Table 1). For example, the shortest O6 ··· H(methyl) contacts are 2.72 and 2.57 Å for the MeO6 isomers of the *R* and *S* enantiomers, respectively, consistent with the latter having the higher strain energy. The methyl ··· H8 contacts in the isomers MeH8 are 2.9–3.4 Å (Table 2), sufficiently short to generate strong cross peaks in the ROESY spectra; these contacts form the basis of the isomer assignment as detailed below. Isomers MeO6 are not expected to give rise to cross peaks between H8 and the axial methyl protons.



0947-6539/02/0823-5488 $ 20.00+.50/0 *Chem. Eur. J.* **2002**, *8*, No. 23

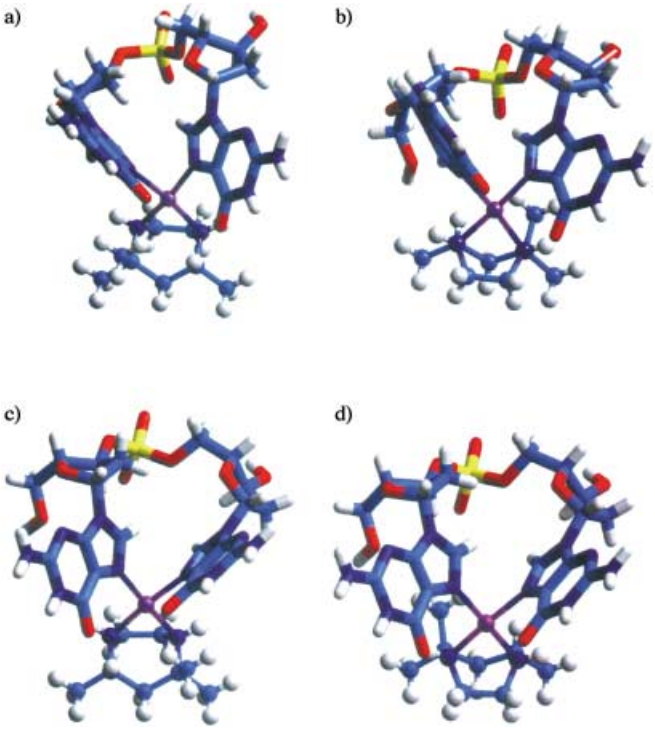


Figure 1. Energy-minimised models of the $HH_1$ rotamers of a) isomer MeO6, [Ptd(GpG){(*R*)-tmdz}], b) isomer MeH8, [Ptd(GpG){(*R*)-tmdz}], c) isomer MeO6, [Ptd(GpG){(*S*)-tmdz}] and d) isomer MeH8, [Ptd(GpG){(*S*)-tmdz}].

Table 2. Short interligand H···H contacts [Å] in the energy-minimised models of the $HH_1$ enantiomers and isomers of [Ptd(GpG)(tmdz)]. Interactions observed in the ROESY spectra are shown in bold.

| | [Ptd(GpG)({(*R*)-tmdz})] | | [Ptd(GpG){(*S*)-tmdz}] | |
|---|---|---|---|---|
| Rotamer | Isomer MeO6 | Isomer MeH8 | Isomer MeO6 | Isomer MeH8 |
| H8a···methyl5** | 4.90 | 6.61 | 7.14 | 6.71 |
| H8a···methyl5* | 4.40 | **3.35** | 5.37 | 2.94 |
| H8a···methyl3* | 7.41 | 3.75 | 6.59 | 4.53 |
| H8a···H8b | 3.06 | **3.17** | 2.74 | **2.53** |
| H8b···methyl5** | 7.49 | 6.03 | 5.42 | 5.83 |
| H8b···methyl5* | 5.41 | **3.12** | 4.82 | **3.23** |
| H8b···methyl3* | 6.85 | 6.46 | 5.97 | 6.41 |

In isomer MeO6 of the *R* enantiomer, the axial methyl group is adjacent to the 5′-O6 which forces the 5′-guanine into an orientation approximately perpendicular to the coordination plane to minimise the contact, and the H8 of the 3′-guanine is disposed into the face of the 5′-guanine (right-handed canting, R2). In isomer MeO6 of the *S* enantiomer, the axial methyl group is adjacent to the 3′-O6 resulting in the 3′-guanine lying approximately perpendicular to the coordination plane and the 5′-H8 being disposed into the face of the 3′-guanine (left-handed canting, L1). In isomers MeH8, interactions between the axial methyl group and the H8 atom result in tilting of the 3′-guanine for the *R* enantiomer and of the 5′-guanine for the *S* enantiomer, forcing them to be disposed into of the face of the 5′- and 3′-guanines, respectively; this gives rise to the same cantings as observed for isomer MeO6 of the same enantiomer. These enantiospecific effects give rise to differences in the NMR spectra of the *R* and *S* enantiomers, and to similarities in the spectra of the two isomers of each enantiomer, as described below. The steric bulk of the tmdz ligand imposes severe constraints on the orientation of the guanine bases, to a significantly greater extent than in other systems studied to date.

**Head-to-tail models**: There are eight forms of the head-to-tail (HT) conformers, because, for each isomer and each enantiomer, either the 5′- or the 3′-guanine can adopt the *syn* conformation giving rise to *anti*,*syn* and *syn*,*anti* or $HT_1$ and $HT_2$ conformers. All eight were subjected to energy minimisation (Figures S3 and S4 in the Supporting Information) and the strain energies are given in Table 1. For the isomers of the *R* enantiomer, the $HT_1$ forms are less stable, because they both have the axial methyl adjacent to an O6 (O6···H 2.40, 2.42 Å). Conversely, for the isomers of the *S* enantiomer, it is the $HT_2$ forms that are destabilised by clashes between these groups (O6···H 2.48, 2.48 Å). Most revealing are the differences in strain energy between the head-to-head to head-to-tail forms; these too are listed in Table 1. For isomer MeO6 of the *R* enantiomer, there is a large decrease in strain energy on going to $HT_2$, as a result of the relieving of the unfavourable contact between the 5′-O6 and the axial methyl group. Conversely, there is an increase in the strain energy on going to the $HT_1$ rotamer of the MeH8 isomer, because this gives rise to a clash between the 5′-O6 and the axial methyl group. Similar changes are observed for the *S* enantiomer, with a large decrease in strain energy on going to $HT_1$ of isomer MeO6 and a small decrease on going to $HT_2$ of isomer MeH8 as O6 to axial methyl repulsions are relieved or produced respectively. Overlaying these changes are a generally lower strain energy for the head-to-tail forms and for the $HT_2$ forms in particular. The $HT_2$ rotamers are generated by rotation of the 5′-guanine and consequently these guanines are usually more mobile. Except where such rotation would give rise to unfavourable contacts, this results in broader peaks in the NMR spectra as outlined below.

**NMR spectroscopy of the d(GpG) adducts**: The one-dimensional, COSY and ROESY $^1$H NMR spectra of the four [Ptd(GpG)(tmdz)] species [bands 1 and 2 from the HPLC separations for each of (*R*)- and (*S*)-tmdz] are given in the Supporting Information (Figures S5–S9). The ROESY spectra showing the correlations between the H8 and tmdz protons are given in Figure 2. Ligand and sugar protons were assigned by using the COSY spectra and the H8 protons were assigned by using the ROESY spectra. The directionality of the dinucleotide was determined by using phosphorus–proton correlation spectroscopy,[36] in which the correlation between the H3a′ and H5b′ protons and the phosphorus allowed complete assignment. Assignments are given in the Supporting Information (Tables S1 and S2).

The primary purpose of the NMR studies was to structurally assign the isomers. In the ROESY spectra of the two band 2 species (Table 3) moderate to weak cross peaks were observed between the signals due to the H8 protons and the axial methyl group protons of the tmdz ligand. No cross peaks due to interactions of the H8 protons with tmdz protons were observed for the band 1 species. There are strong H8···H8

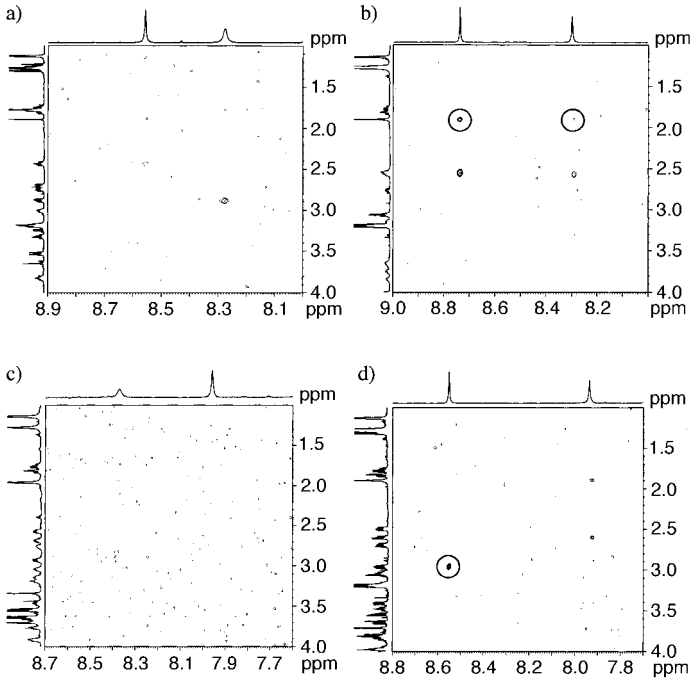


Figure 2. ROESY spectra showing the H8/tmdz regions for a) band 1, [Ptd(GpG){(*R*)-tmdz}], b) band 2, [Ptd(GpG){(*R*)-tmdz}], c) band 1, [Ptd(GpG){(*S*)-tmdz}], and d) band 2, [Ptd(GpG){(*S*)-tmdz}]. Cross peaks between the resonances due to the H8 atoms and the axial methyl group are circled.

Table 3. Relative intensities of the ligand···H8 ROESY cross peaks in the band 2 spectra.

| [Ptd(GpG){(*R*)-tmdz}] | Relative strength of interaction[a] | [Ptd(GpG){(*S*)-tmdz}] | Relative strength of interaction[a] |
|---|---|---|---|
| H8a···methyl5* | M | H8a···methyl5* | W |
| H8b···methyl5* | M | | |

[a] M = medium, W = weak.

cross peaks in the spectra of the band 2 species, indicating that they predominantly adopt a HH conformation. On the basis of these cross peaks it is established that the band 2 species have the isomer MeH8 geometry in which, for the $HH_1$ conformer, the axial methyl group is disposed on the same side of the coordination plane as the H8 protons. By inference, the band 1 species have the isomer MeO6 geometry. In the case of isomer MeH8 (band 2) of the *R* enantiomer, a ROESY cross peak was observed between the 3′-H8 and the axial methyl group as well as a weaker cross peak between this methyl group and the 5′-H8. For the same isomer of the *S* enantiomer, only a cross peak between the 5′-H8 and the axial methyl group of tmdz was observed. These cross peaks are consistent with the contacts seen in the models of the isomers MeH8 of the two enantiomers (Figure 1, Table 2), because on going from the *R* to the *S* enantiomer, the axial methyl group moves from the 3′-side to the 5′-side. It may also be relevant that the stronger ROESY cross peak for each enantiomer is from the axial methyl group of the tmdz ligand to the H8 of the guanine, which is prevented from rotating to a *syn* orientation by the axial methyl group.

The H8 regions of the one-dimensional spectra reveal a number of differences between the isomers and enantiomers. The shifts of the resonances due to the H8 protons range from $\delta = 7.93$ to 8.74 ppm (Table 4), similar to the range observed for many d(GpG) complexes. For both isomers formed by the

Table 4. H8 chemical shifts [ppm] for the HPLC fractions of the enantiomers of [Ptd(GpG)(tmdz)].

| Rotamer | [Ptd(GpG){(*R*)-tmdz}] Isomer MeO6 | [Ptd(GpG){(*R*)-tmdz}] Isomer MeH8 | [Ptd(GpG){(*S*)-tmdz}] Isomer MeO6 | [Ptd(GpG){(*S*)-tmdz}] Isomer MeH8 |
|---|---|---|---|---|
| H8a (5′) | 8.28 | 8.30 | 8.37 | 8.55 |
| H8b (3′) | 8.56 | 8.74 | 7.96 | 7.93 |

*R* enantiomer, the H8 shifts of the 3′-guanine bases are further downfield than those of the 5′-guanine bases, but the reverse is true for both isomers formed by the *S* enantiomer. Kozelka and co-workers have proposed that the shifts of the H8 proton signals depend on the orientations of the guanine bases with respect to one another.[37, 38] Marzilli et al. have refined these proposals, suggesting that mobility of the guanine bases can play a significant role in determining the H8 shifts.[39] Both groups agree that if the H8 of the 3′-guanine is tilted into the "face" of the resonance of the 5′-guanine (R2 canting), then the 5′-H8 signal is expected to be further downfield than the resonance of the 3′-guanine H8. Conversely, if the H8 of the 5′-guanine is tilted toward the face of the 3′-guanine (L1 canting), the resonance of the 3′-H8 signal is expected to be further downfield than that of the 5′-H8. Inspection of the models in Figure 1 reveals that the axial methyl group interacts closely with either O6 or H8 influencing the canting of the adjacent base. On going from the *R* to the *S* enantiomer, the methyl group moves from being adjacent to the 3′ end to the 5′, or vice versa, depending on the isomer. As a consequence both isomers of the *R* enantiomer adopt R2 canting, while those of the *S* enantiomer adopt the L1 canting, evidently generating the enantiospecific effect on the H8 shifts. However, the pattern of shifts observed is opposite to that expected for these cantings.[37, 38] It is not evident why this is the case, but, as noted above, an unusual feature of the tmdz ligand is the limitation it imposes on the rotation of the guanine bases. It may be that this restricted rotation results in a different shift pattern to that observed for more flexible systems and Marzilli et al. have suggested that such factors can be important.[39]

The spectra of band 1 and band 2 differ further in that for band 1, one peak, that due to the 5′-H8, is broadened with respect to the other, whereas for band 2, both peaks are sharp. Additionally, there are no H8···H8 cross peaks in the band 1 ROESY spectra. These results are suggestive of the 5′-guanine in the band 1 species being more mobile and perhaps spending a substantial portion of its time in the *syn* orientation, giving rise to the $HT_2$ configuration. Band 1 corresponds to isomer MeO6, which is the most strained in the $HH_1$ configuration, and, therefore, it is not surprising that there is an increased tendency to adopt a HT configuration. Also, the broad H8 peaks correspond the guanine bases that interact unfavourably with the axial methyl group and are



0947-6539/02/0823-5490 $ 20.00+.50/0 *Chem. Eur. J.* **2002**, *8*, No. 23

therefore more likely to undergo rotation to the *syn* orientation to relieve the O6 $\cdots$ axial methyl interaction. Indeed, there is a general correlation between the broadness of the H8 peaks and the difference between strain energies of the relevant head-to-head and head-to-tail rotamers.

**52-mer binding**: Each of the enantiomers of [$PtCl_2$(tmdz)] was treated separately with the 52-mer oligonucleotide and the reaction mixtures were enzymatically digested. HPLC analysis of the products revealed only two peaks due to platinated products in each case. Expanded HPLC chromatograms and platinum profiles are shown in Figure 3. The identity of each

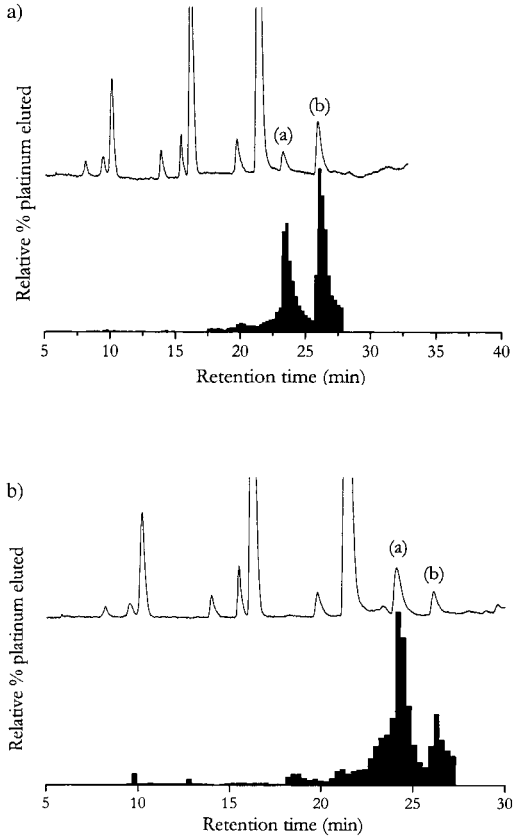


Figure 3. HPLC chromatogram of products and platinum profile of digestion products for a) [Pt(52-mer){(*R*)-tmdz}] and b) [Pt(52-mer){(*S*)-tmdz}]. Peaks a correspond bifunctional adducts and peaks b to monofunctional adducts.

of the peaks was established both by spiking with standards and by removing the platinum with thiourea; the resulting mixtures were subjected to chromatography again to determine the identity of the nucleoside or dinucleotide (Figures S5 and S6 in the Supporting Information). In each case, the first of the peaks was found to be due to band 2 (isomer MeH8) of the d(GpG) complex, [Ptd(GpG)(tmdz)], and the second was due to one or more of the species ([PtX(dG)(tmdz)]) that arise from the monofunctional adducts on the DNA. No significant trace of isomer 1 of the d(GpG) complex observed for either enantiomer, indicating that complete stereoselectivity or stereospecificity in the formation of the bifunctional adduct was achieved. Stereospecificity, or at least high stereoselectivity, was anticipated because of the steric bulk of the trimethylpropylene chain of the tmdz ligand. In the case of isomer MeO6, the molecular models of {Pt(tmdz)} bound to a dG8:dC8 8-mer duplex (Figure 4) reveal that the methyl groups make many close contacts with the DNA. The most pronounced of these contacts are between the O6 atoms and the trimethylpropylene chain of the tmdz ligand. For the *R* enantiomer, there are three 2.7 Å contacts: between the axial methyl group and both O6 atoms and between the methine proton of tmdz and the 3′O6. As a consequence the 3′N7-Pt-NH angle is opened to 112.9° in order to partially relieve the stresses of these contacts. For the *S* enantiomer, there is only a single very destabilising contact of 2.4 Å, between the axial methyl group and the 3′O6, and the 3′N7-Pt-NH angle is opened even more to 113.7°. These strongly repulsive interactions would, for both enantiomers, have the effect of reducing the likelihood of closure from the monofunctional to the bifunctional adduct. In contrast, there is only a single O6 $\cdots$ H contact of 2.8 Å in the *R* enantiomer of isomer MeH8 and of 2.6 Å in the *S* enantiomer of this isomer. The N7-Pt-NH angles are not significantly distorted from their normal values in the isomer MeH8 models, consistent with the lack of steric clashes. Similar results were observed in models of the *R* enantiomer bound to the d($C_1A_2T_3G_4G_5T_6A_7C_8$)-3′:3′-d($G_{16}T_{15}A_{14}C_{13}$-$C_{12}A_{11}T_{10}G_9$)-5′ sequence, with the addition of some close, but not strongly destabilising, contacts (2.6–2.7 Å) with the methyl groups of the thymines flanking the GpG site. Thus, the appearance of only isomer MeH8 of the bifunctional adduct in the digests of the reaction with the 52-mer is consistent with the trimethylpropylene chain, and the axial methyl group in particular, exerting steric control over the formation of this adduct.

The observation of a substantial amount of monofunctional adduct is also consistent with the tmdz ligand exerting a steric control that operates by preventing closure to the bifunctional adduct. Enantioselectivity is observed in that the *R* enantiomer forms more monofunctional adducts than bifunctional (59:41), whereas the *S* enantiomer forms more bifunctional adducts (27:73). The axial methyl group is primarily responsible for the observed steric effects, and it changes position on going from the *R* to the *S* enantiomer, so sterically induced enantioselectivity is not unexpected. For the *R* enantiomer, the amount of monofunctional adduct exceeds the amount of bifunctional adduct, whereas for the *S* enantiomer, the monofunctional adducts are formed to a much smaller extent than the bifunctional adduct. This enantioselectivity must arise at the level of monofunctional adduct formation, because it is related to the amount of monofunctional adducts that do not close to bifunctional adducts. Given that the reactions were allowed to proceed for seven days at 37 °C, this can be taken to be only those that are prevented from closing by steric clashes.

The origin of this enantioselectivity was investigated by molecular modelling with an approach described previously.[40] Monofunctional adducts have a pronounced influence on the conformation of the flanking bases and, consequently, these bases have the potential to influence the formation of the monofunctional adducts. Therefore, in modelling these

  0947-6539/02/0823-5491 $ 20.00+.50/0 

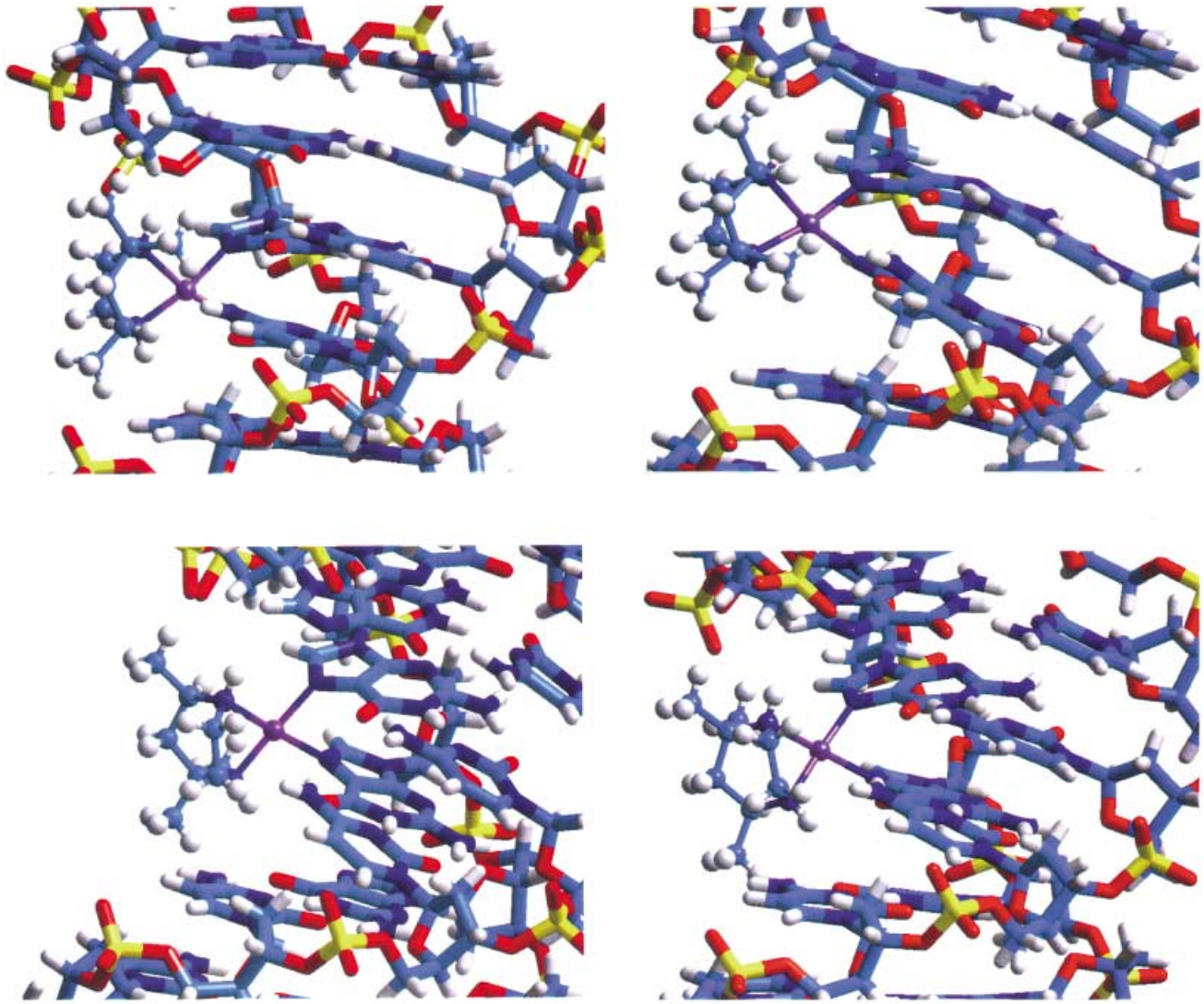

Figure 4. Left-hand side: Molecular modelling representation of the two bifunctional isomers formed in the reactions of [$PtCl_2${(*R*)-tmdz}] with a dG8:dC8 sequence. Top: Model MeO6. Bottom: Model MeH8. Right-hand side: Molecular modelling representation of the two bifunctional isomers formed in the reactions of [$PtCl_2${(*S*)-tmdz}] with a dG8:dC8 sequence. Top: Model MeO6. Bottom: Model MeH8.

adducts, a sequence the same as that containing the GpG sites in the 52-mer was used (5′-CATGGTAC-3′:5′-GTACCATG-3′). A number of rotamers can form when the enantiomers of [$PtCl_2$(tmdz)] bind monofunctionally to either guanine of this sequence. These rotamers are best visualised by dividing the space around the N7 of the guanine into the four quadrants identified by the position of the chlorine ligand relative to the plane containing the O6, and labelled A, B, C or D, in which quadrant A has the chlorine lying toward and above (5′ side) the O6 and B, C and D are related by clockwise rotations of 90° from this position.[40] Taking into account the four rotamers, two enantiomers and the 5′- and 3′-guanine bases, there are 32 possible monofunctional adduct models. All were generated and subjected to energy minimisation, but not all yielded stable minima because in some cases the steric clashes were so severe that interconversion to other rotamers occurred. The preferred rotamer, taken as the one that induced the least distortion to the structures of the DNA and the complex, was found be rotamer A, and this was successfully energy minimised for all combinations of enantiomer and guanine. An example of rotamer A is shown in Figure 5. For the A rotamers of each of the *R* and *S* enantiomers, the two preferred monofunctional adducts have N1 (the amine adjacent to the axial methyl group) *trans* to the 3′-guanine and *cis* to the 5′-guanine. All four of these favoured models have the tmdz ligand lying unencumbered in the major groove of the DNA with no unfavourable interactions with the DNA. However, they differ in that the two favoured isomers of the monofunctional adduct formed by the *R* enantiomer are not able to ring close, because they would give rise to the disfavoured isomer MeO6 of the bifunctional adduct, whereas those of the *S* enantiomer give rise to isomer MeH8 and are able to ring close. On this basis, the *R* enantiomer would be expected to form a higher proportion of the monofunctional adducts that are unable to close, and the *S* enantiomer more of those that can close. This is in accord with the higher proportion of monofunctional adducts observed in the enzymatic digestion experiments involving the *R* enantiomer, and the higher proportion of bifunctional adducts for the *S* enantiomer.



0947-6539/02/0823-5492 $ 20.00+.50/0 *Chem. Eur. J.* **2002**, *8*, No. 23

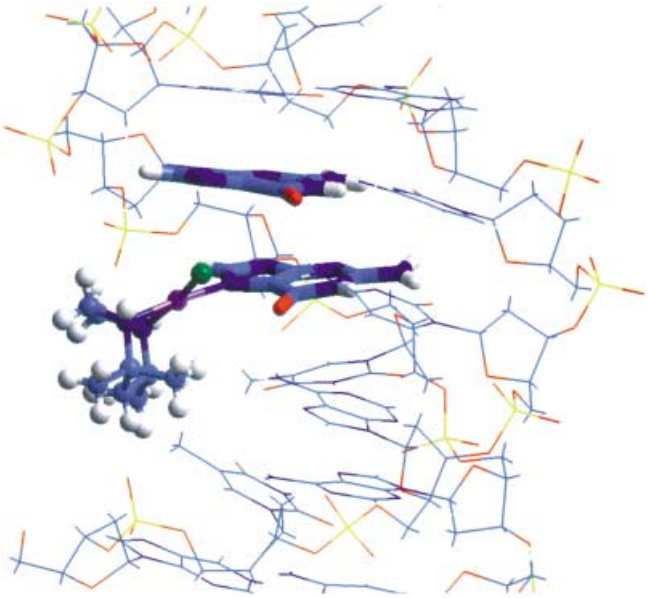

Figure 5. Molecular modelling representation of rotamer A of the monofunctional adduct in which [$PtCl_2$\{(*R*)-tmdz\}] to the 3′-guanine of a GpG pair with the axial methyl group cis to the coordinated N7. The tmdz ligand can be seen to sit unencumbered in the major groove.

## Conclusion

The steric bulk of the tmdz ligand is shown to have pronounced effects on both the adducts with the d(GpG) dinucleotide and the binding to duplex oligonucleotides. The rotation of the guanine bases in the dinucleotide complexes is restricted by the tmdz ligand; this gives rise to enantiospecific trends in NMR chemical shifts and to differences in the broadness of the H8 peaks. ROESY contacts between the tmdz and d(GpG) ligands readily identified the isomers. Interactions between the tmdz and duplex DNA gave rise to stereospecificity in the formation of stereoisomers of the bifunctional adducts and enantioselectivity in the formation of monofunctional adduct.

## Acknowledgements

We thank the Australian Research Council and the Sydney University Cancer Research Fund for financial support.

[1] E. R. Jamieson, S. J. Lippard, *Chem. Rev.* **1999**, *99*, 2467–2498.
[2] H. Harder, B. Rosenberg, *Int. J. Cancer* **1970**, *6*, 207–216.
[3] J. A. Howle, G. R. Gale, *Biochem. Pharmacol.* **1970**, *19*, 2757–2762.
[4] J. J. Roberts, A. J. Thomson, *Prog. Nucleic Acid Res. Mol. Biol.* **1979**, *22*, 71–133.
[5] A. Pinto, S. J. Lippard, *Biochim. Biophys. Acta* **1985**, *780*, 167–180.
[6] J. Zehnulova, J. Kasparkova, N. Farrell, V. Brabec, *J. Biol. Inorg. Chem.* **2001**, *276*, 22191–22199.
[7] T. D. McGregor, A. Hegmans, J. Kasparkova, K. Neplechova, O. Novakova, H. Penazova, O. Vrana, V. Brabec, N. Farrell, *J. Biol. Inorg. Chem.* **2002**, *7*, 397–404.
[8] J. Reedijk, *Inorg. Chim. Acta* **1992**, *198–200*, 873–881.
[9] M. S. Davies, J. W. Cox, S. J. Berners-Price, W. Barklage, Y. Qu, N. Farrell, *Inorg. Chem.* **2000**, *39*, 1710–1715.
[10] M. S. Davies, S. J. Berners-Price, T. W. Hambley, *Inorg. Chem.* **2000**, *39*, 5603–5613.
[11] J. W. Cox, S. J. Berners-Price, M. S. Davies, N. Farrell, Y. Qu, *J. Am. Chem. Soc.* **2001**, *123*, 1316–1326.
[12] T. W. Hambley, *J. Chem. Soc. Dalton Trans.* **2001**, 2711–2718.
[13] A. Eastman, *Biochemistry* **1982**, *21*, 6732–6736.
[14] A. Eastman, *Biochemistry* **1983**, *22*, 3927–3933.
[15] A. Eastman, *Pharmacol. Ther.* **1987**, *34*, 155–166.
[16] A. M. J. Fichtinger-Schepman, P. H. M. Lohman, J. Reedijk, *Nucleic Acids Res.* **1982**, *10*, 5345–5356.
[17] A. M. J. Fichtinger-Schepman, J. L. van der Veer, J. H. J. den Hartog, P. H. M. Lohman, J. Reedijk, *Biochemistry* **1985**, *24*, 707–713.
[18] T. W. Hambley, E. C. H. Ling, S. O'Mara, M. J. McKeage, P. J. Russell, *J. Biol. Inorg. Chem.* **2000**, *5*, 675–681.
[19] T. W. Hambley, E. C. H. Ling, V. P. Munk, M. S. Davies, *J. Biol. Inorg. Chem.* **2001**, *7*, 534–542.
[20] J. F. Hartwig, S. J. Lippard, *J. Am. Chem. Soc* **1992**, *114*, 5646–5654.
[21] Y. Chen, J. A. Parkinson, Z. Guo, T. Brown, P. J. Sadler, *Angew. Chem.* **1999**, *111*, 2192–2196; *Angew. Chem. Int. Ed.* **1999**, *38*, 2060–2063.
[22] G. L. Cohen, J. A. Ledner, W. R. Bauer, H. M. Ushay, C. Caravana, S. J. Lippard, *J. Am. Chem. Soc.* **1980**, *102*, 2487–2488.
[23] K. Inagaki, K. Sawaki, *Chem. Pharm. Bull.* **1995**, *43*, 183–188.
[24] V. P. Munk, R. R. Fenton, T. W. Hambley, *Polyhedron* **1999**, *18*, 1039–1043.
[25] A. Eastman, *Biochemistry* **1985**, *24*, 5027–5032.
[26] T. W. Hambley, E. C. H. Ling, B. A. Messerle, *Inorg. Chem.* **1996**, *35*, 4663–4668.
[27] A. Eastman, *Biochemistry* **1986**, *25*, 3912–3915.
[28] A. Eastman, M. M. Jennerwein, D. L. Nagel, *Chem.-Biol. Interact.* **1988**, *67*, 71–80.
[29] HyperCube, HyperChem, 4.5 ed., **1995**.
[30] T. W. Hambley, MOMECSG-95, University of Sydney, **1996**.
[31] T. W. Hambley, *Inorg. Chem.* **1988**, *28*, 1073–1077.
[32] T. W. Hambley, *Inorg. Chem.* **1991**, *30*, 937–942.
[33] T. W. Hambley, *Inorg. Chem.* **1998**, *37*, 3767–3774.
[34] S. O. Ano, F. P. Intini, G. Natile, L. G. Marzilli, *J. Am. Chem. Soc.* **1998**, *120*, 12017–12022.
[35] C.-L. Teo, R. R. Fenton, P. Turner, T. W. Hambley, *Aust. J. Chem.* **1998**, *51*, 977–984.
[36] G. Bodenhausen, D. J. Ruben, *Chem. Phys. Lett.* **1980**, *69*, 185–188.
[37] J. Kozelka, M.-H. Fouchet, J.-C. Chottard, *Eur. J. Biochem* **1992**, *205*, 895–906.
[38] D. Lemaire, M.-H. Fouchet, J. Kozelka, *J. Inorg. Biochem.* **1994**, *53*, 261–271.
[39] L. G. Marzilli, S. O. Ano, F. P. Intini, G. Natile, *J. Am. Chem. Soc.* **1999**, *121*, 9133–9142.
[40] F. Reeder, Z. Guo, P. S. Murdoch, A. Corazza, T. W. Hambley, S. J. Berners-Price, J.-C. Chottard, P. J. Sadler, *Eur. J. Biochem.* **1997**, *249*, 370–382.

Received: June 27, 2002 [F4210]